Chinese Journal of
POLYMER SCIENCE

RESEARCH ARTICLE

https://doi.org/10.1007/s10118-024-3110-z
Chinese J. Polym. Sci. **2024**, *42*, 926–935

Holographic Polymer Nanocomposites with High Refractive Index Modulation by Doping Liquid Crystal E6M

Meng-Yun Wang[a], Yue Zhang[a], Dan Wang[a], Ming Yao[a], Yi-Xuan Wang[a], Xing-Ping Zhou[a,b,c], Hai-Yan Peng[a,b,c*], and Xiao-Lin Xie[a,b,c]

[a] *Key Laboratory of Material Chemistry for Energy Conversion and Storage, Ministry of Education, School of Chemistry and Chemical Engineering, Huazhong University of Science and Technology, Wuhan 430074, China*
[b] *State Key Laboratory of Materials Processing and Die & Mould Technology, Huazhong University of Science and Technology, Wuhan 430074, China*
[c] *National Anti-counterfeit Engineering Research Center, Huazhong University of Science and Technology, Wuhan 430074, China*

Electronic Supplementary Information

Abstract Holographic optical elements (HOEs) based on polymer composites have become a research hot spot in recent years for augmented reality (AR) due to the significant improvement of optical performance, dynamic range, ease of processing and high yield rate. Nevertheless, it remains a formidable challenge to obtain a large field of view (FOV) and brightness due to the limited refractive index modulation. Herein, we report an effective method to tackle the challenge by doping an epoxy liquid crystal termed E6M, which enables a large refractive index modulation of 0.050 @ 633 nm and low haze of 5.0% at a doping concentration of 5 wt%. This achievement may be ascribed to the improved molecular ordering of liquid crystals within the holographic polymer composites. The high refractive index modulation can endow transmission-type holographic polymer composites with a high diffraction efficiency of 96.2% at a small thickness of 5 μm, which would promise the design of thin and lightweight AR devices.

Keywords Polymer nanocomposites; Holography; AR/VR; Refractive index modulation; Liquid crystal

Citation: Wang, M. Y.; Zhang, Y.; Wang, D.; Yao, M.; Wang, Y. X.; Zhou, X. P.; Peng, H. Y.; Xie, X. L. Holographic polymer nanocomposites with high refractive index modulation by doping liquid crystal E6M. *Chinese J. Polym. Sci.* **2024**, *42*, 926–935.

INTRODUCTION

With the rapid development of high-speed communications and mobile computing, augmented reality (AR) is blazing as the next generation display platform that can deepen the human-machine interactions. As a matter of fact, AR technologies have been of immense utility in a broad range of fields such as healthcare, industry incubation, immersive teaching and games.[1,2] Optical elements for reshaping the light path within AR setups are indispensable and can significantly affect the ultimate imaging prowess. However, traditional optical elements like freeform prisms, off-axis aspheric mirrors and birdbath, are subject to fundamental physical constraints when it comes to complex design and machining on a large scale.[3,4] Alternatively, holographic optical elements (HOEs) have proved to bring fresh vitality.[5,6] The combination of HOEs with waveguide elements can not only eliminate the cumbersome and intricate lens groups, but can also provide more design freedom to adjust the field of view (FOV) and eye box. In addition, such a combination can also improve the optical efficiency and thus provide a high brightness even with a low illumination intensity.[7,8] This is of vital significance for reducing power consumption and miniaturing the light source. Unfortunately, the refractive index modulation (n_1) of current HOEs generally remains small, which would consequently restrict the FOV and diffraction efficiency.[7,9–12] In addition, under such a condition, a thick HOE must be used for ensuring a high diffraction efficiency and display brightness, which would also hamper endeavors to fabricate thin and lightweight AR setups. Clearly, it is in an urgent need to develop high n_1 materials to ensure high-performance HOEs.

In response to the above challenge, holographic polymer nanocomposites, particularly those containing liquid crystals (LCs),[13–19] have recently garnered significant interests as a noteworthy type of HOEs.[20–25] This is because the introduction of LCs can not only offer a high n_1, but also can impart exceptional susceptibility to external fields and attractive processing feasibility.[23,26–35] The most appealing example was reported by DigiLens in which the n_1 could be as high as 0.15 and thus the FOV approached 50° diagonal.[36,37] However, the formulations are undisclosed probably due to the commercial interests. In 2023, Ni *et al*. also reported a high-performance HOE with a high n_1 of 0.08, which offered a FOV of 30°

* Corresponding author, E-mail: hypeng@hust.edu.cn
Special Issue: Functional Polymer Materials
Received January 4, 2024; Accepted February 21, 2024; Published online April 10, 2024

diagonal.[7] Despite these inspiring achievements, there is still lack of versatile approach to boost the n_1. Though further increasing the refractive index of LCs might be a reasonable approach to improve the n_1 and thus the FOV and brightness, significant light scattering loss would arise due to increased mismatch of refractive index between the polymer-rich and LC-rich regions.[20,38,39] Under such a condition, the haze would be increased, leading to decreased optical transparency and poor quality of AR display.

Herein, we reported a viable approach to boosting the n_1 of holographic polymer composites while decreasing the haze by doping an epoxy LC termed E6M. Interestingly, the n_1 could reach 0.050 @ 633 nm and the haze decreased to 5.0%. This achievement may be ascribed to the fact that the E6M can facilitate the LC ordering within holographic polymer composites (Fig. 1).

EXPERIMENTAL

Materials

Chemicals used for synthesizing LC E6M and MPEB

Sodium hydroxide (purity: 99.5%) was obtained from TCI Chemicals. Ethyl acetate (purity: 99.8%), anhydrous ethanol (purity: 99.7%), potassium iodide (KI, purity: 99%) and *p*-hydroxybenzoic acid (purity: 99%) were received from Innochem, China. 6-Bromo-1-hexene (purity: 95%), *n*-hexane (purity: 98%), methyl hydroquinone (purity: 99%) and *p*-dimethylaminopyridine (DMAP, purity: 99%) were purchased from Aladdin, China. Dichloromethane (CH_2Cl_2, purity: 99.8%), potassium hydroxide (KOH, purity: 99%) and hydrochloric acid (HCl, concentration: 37 vol%) were acquired from Acros Organics, Belgium. Sodium chloride (NaCl, purity: 99.5%), sodium sulfite (purity: 98%), sodium carbonate anhydrous (Na_2CO_3, purity: 99.9%) and sodium sulfate (Na_2SO_4, purity: 99%) were received from Sigma-Aldrich, United States. Magnesium sulfate anhydrous (purity: 97%), 3-chloroperoxybenzoic acid (mCPBA, purity:75%) and *N*,*N*'-dicyclohexylcarbodiimide (DCC, purity: 99%) were supplied by Macklin, China.

Commercial LC for holographic recording

The nematic LC P0616A ($n_{e(589nm,20℃)}$=1.72, $n_{0(589nm,20℃)}$=1.52) was supplied by Shijiazhuang Chengzhi Yonghua Display Materials Co., Ltd., China.

Monomers for holographic recording

N,*N*-dimethylacrylamide (DMAA, purity>99%) was purchased from J&K Scientific, China. The multifunctional acrylate monomer 6361-100 was donated by Eternal Materials Co., Ltd., China.

Photoinitiating system

3,3'-Carbonylbis(7-diethylaminocoumarin) (KCD, purity: 99%) as the photosensitizer was received from Acros Organics, Belgium. *N*-phenylglycine (NPG, purity >97%) as the co-initiator was obtained from TCI Chemicals. The combination of KCD with NPG led to the formation of "photoinitibitor" with both the initiation and inhibition functions.[27]

LC cells

ITO cells with a gap of 5 μm was purchased from Hunan Future Electronics Technology, Co., Ltd, China.

Characterization Methods

Molecular structures were characterized using nuclear magnetic resonance spectroscopy (NMR, 400 MHz, Ascend, Bruker, Germany). Molecular mass was acquired on the high-resolution mass spectrometry (HRMS, 5800, AB SECIX, United States). LC textures were captured using polarized optical microscopy (POM, Axio Scope. A1, Carl Zeiss, Germany). Heating was implemented at a ramp rate of 3 °C·min^{-1} from 25 °C to 170 °C while the cooling was exerted at a ramp rate of 2 °C·min^{-1}. Phase tran-

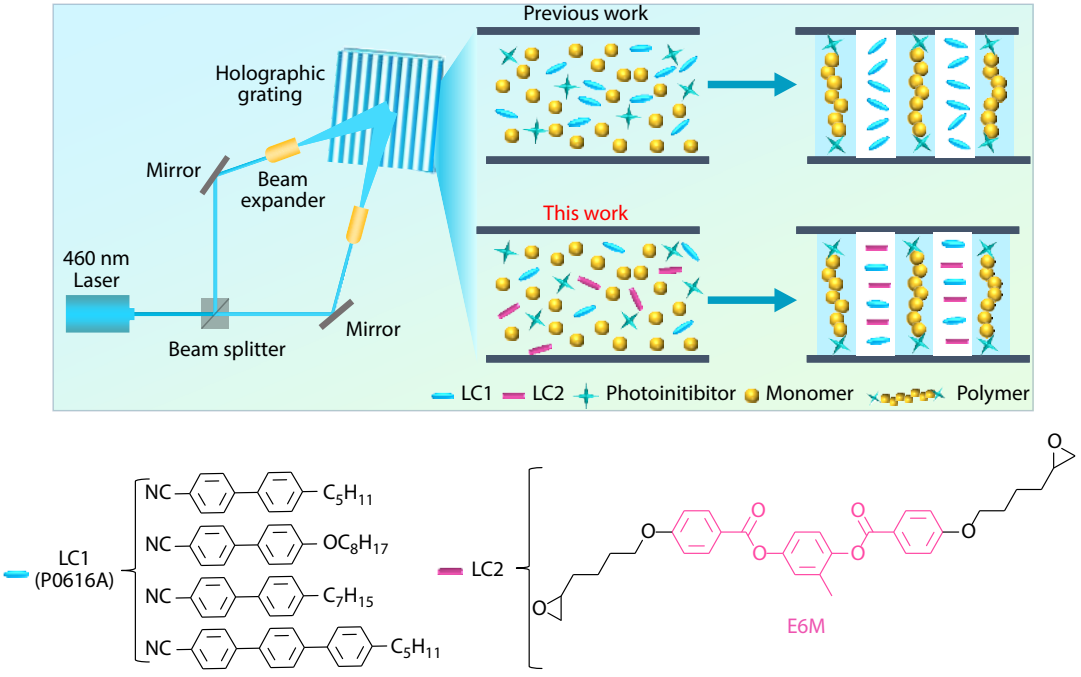

Fig. 1 Schematic illustration on the construction of high-performance LC-based holographic polymer nanocomposites by doping E6M. P0616A was commercially available LC in nematic phase.

sition temperatures were analyzed on a differential scanning calorimeter (DSC, Q2000, TA, United States). Cooling and heating were implemented at a ramp rate of 5 °C·min^{-1} between −20 and 180 °C. For the holographic polymer nanocomposites with grating structures, the diffraction efficiency and electro-optic response were monitored using an LCD display parameter tester (LCT-5016C, North LC Engineering Research and Development Center, China. Probe wavelength: 633 nm), the haze was characterized using hazemeter (WGT-S, Shanghai Shengguang Instrument Co., Ltd, China), and the micromorphology was analyzed using atomic force microscopy (AFM, SPM-9700, Shimadzu, Japan) in the tapping mode. The LCs were removed by soaking the gratings in hexane for 3 days before characterization. Photopolymerization kinetics was analyzed using Fourier transform infrared spectroscopy (FTIR, V80, Bruker, Germany) when *in situ* shining light (wavelength: 460 nm, intensity: 2.0 mW·cm^{-2}, time: 500 s). Temperature-dependent wide-angle X-ray scattering (T-WAXS) characterizations at 20, 100 and 180 °C, respectively, were performed at Soochow University on a scattering instrument (SAXSess mc^2, Anton paar, Austria) with a temperature controller (TCS 300, Anton paar, Austria).

Chemical Synthesis

In this work, E6M, namely 2-methyl-1,4-phenylenebis(4-(2-(oxiran-2-yl)ethoxy)benzoate) was synthesized by referencing the reported method.[40,41] As shown in Scheme 1, E6M was synthesized in three-steps, wherein 2-methyl-1,4-phenylene bis(4-(allyloxy)benzoate) (shortened as MPEB) was one of the intermediates.

Synthesis of 4-allyloxybenzoic acid

To start with, CH_3OH (100 mL), H_2O (24 mL), KOH (20.0 g, 357 mmol), *p*-hydroxybenzoic acid (19.0 g, 137 mmol) and KI (0.2 g, 1.2 mmol) were added to a 500 mL round-bottom flask and stirred at 0 °C for 30 min. Following, 6-bromo-1-hexene (19.4 mL, 145 mmol) was added dropwise. Subsequently, the mixture was heated up to 80 °C and refluxed for 12 h to complete the reaction. After cooling down to room temperature, the pH value of the mixture was adjusted to 3 by adding HCl solution (concentration: 10 vol%) dropwise. The product was obtained *via* precipitation from the original solution as white color solid (yield: 90%).

Synthesis of MPEB

4-Allyloxybenzoic acid (9.7 g, 44.4 mmol), methylhydroquinone (2.4 g, 19.3 mmol), DMAP (0.4 g, 3.3 mmol) and distilled CH_2Cl_2 (200 mL) were added into a 500 mL round-bottom flask and stirred at 25 °C for 30 min. Afterwards, DCC was added dropwise. After reacting for 24 h at room temperature, the mixture was filtered to remove the residue, and the filtrate was further purified by column chromatography using CH_2Cl_2 as the eluent and finally precipitated in ethyl acetate as white color solid (yield:78%).

Synthesis of E6M

MPEB (5.0 g, 9.4 mmol) and distilled CH_2Cl_2 (120 mL) were added to a 250 mL round-bottom flask. Then, mCPBA (4.83 g, 20.8 mmol) was added dropwise under continuous stirring. After reacting for 3 days at room temperature, the insoluble matter was filtered out, and the residual mixture was extracted with CH_2Cl_2 for three times. The combined organics were washed by aqueous solutions with 10.0 wt% Na_2SO_3, 10.0 wt% $NaHCO_3$ and saturated sodium chloride, respectively. The organic layer was collected and dried with anhydrous Na_2SO_4, and then concentrated *via* vacuum evaporation. The obtained crude product was recrystallized with ethyl acetate to produce white color solid (yield: 42%).

Holographic Recording

The structures of LC-based holographic polymer composites are in periodic, consisting of alternate polymer-rich and LC-rich phases. To generate such periodic structures, a homogeneous mixture of monomers, LCs and photoinitiating systems was sandwiched inside the ITO cells, and then exposed by two coherent laser beams from the same side.[38,42] The laser wavelength was 460 nm ($\lambda_{writing}$), and the external angle of these two beams was set as ~38° (θ_{set}), which thus could create transmission gratings in a period of about 700 nm according to the Bragg Law:[28]

$$\Lambda = \frac{0.5\lambda_{writing}}{\sin\left(\frac{\theta_{set}}{2}\right)} \quad (1)$$

where $\lambda_{writing}$ is laser wavelength, θ_{set} is the external angle of these two beams, and Λ is grating period. During holographic recording, the intensity of each beam was optimized as 1 mW·cm^{-2} while the exposure time was 30 s. After holographic recording, the composite gratings were post-cured by UV light (365 nm, 100 mW·cm^{-2}, 5 min) to solidify the grating structure.[43] To avoid overmodulation, the grating thickness

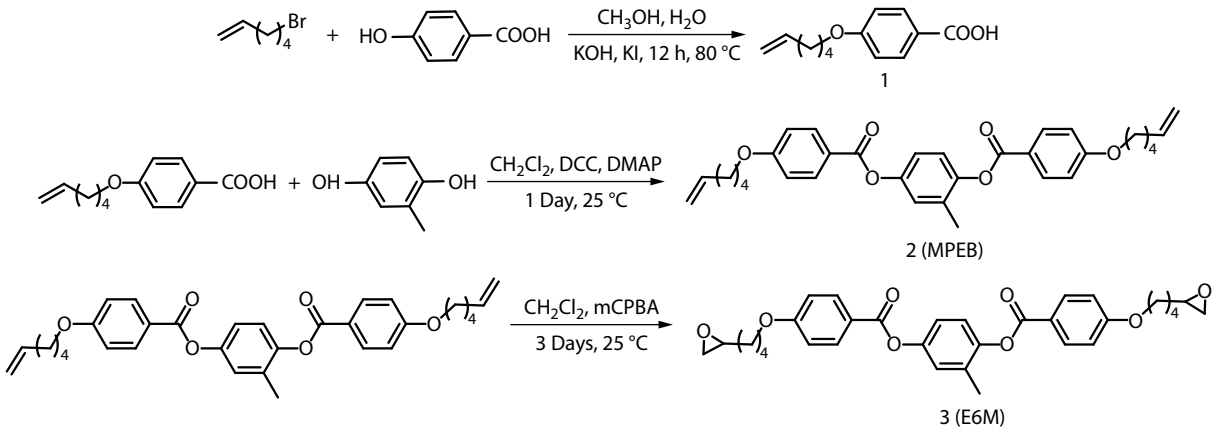

Scheme 1 Synthetic route to E6M.

https://doi.org/10.1007/s10118-024-3110-z

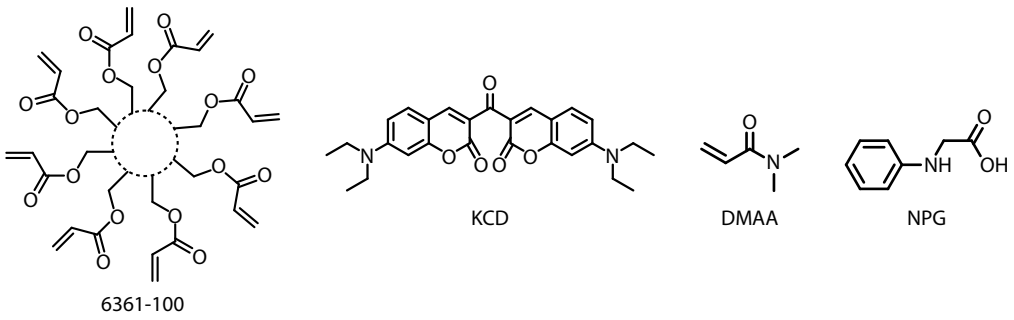

Scheme 2 Schematic illustration of 6361-100, KCD, DMAA, NPG.

was controlled to be 5 μm.

The composite gratings were formed *via* periodic photopolymerization induced phase separation,[13,44] where the photoinitiating system absorbed laser energy, produced radicals and initiated the photopolymerization in the bright region, while the LC molecules were squeezed into the dark regions due to the change of the chemical potential.[32,45,46] To obtain well-defined gratings, the hyperbranched monomer 6361-100 and monofunctional monomer DMAA were utilized as previously optimized (Scheme 2 and Table 1). A monochromatic "photoinitibitor" composed of KCD and NPG was employed as the photoinitiating system which could efficiently regulate the phase separation structures *via* the synergy of the simultaneously generated photoinitiation and inhibition functions.[27,47]

Table 1 Holographic formulations by weight percentage.

Entry	DMAA/6361-100 (2/1)	P0616A	E6M
1#	70.0	30.0	0
2#	70.0	27.5	2.5
3#	70.0	25.0	5.0
4#	70.0	22.5	7.5
5#	70.0	20.0	10.0
6#	70.0	15.0	15.0

RESULTS AND DISCUSSION

LC Characteristics of E6M

LC characteristics of E6M can be characterized by POM and DSC after chemical identification with NMR and HRMS (Figs. S1 and S2 in the electronic supplementary information, ESI). Before POM and DSC characterizations, thermogravimetric analysis (TGA) was exerted to evaluate the thermal stability of E6M, which indicates a high thermal stability up to 374 °C (Fig. S5 in ESI). As shown in Figs. 2(a)–2(c), birefringent patterns become more significant when heating from 25 °C to 89 °C and then faded off at 167 °C. The textures at 89 °C looked schlieren, implying the formation of nematic LC phase, in consistent with previous reports.[31,41] Upon cooling, the birefringent patterns come out

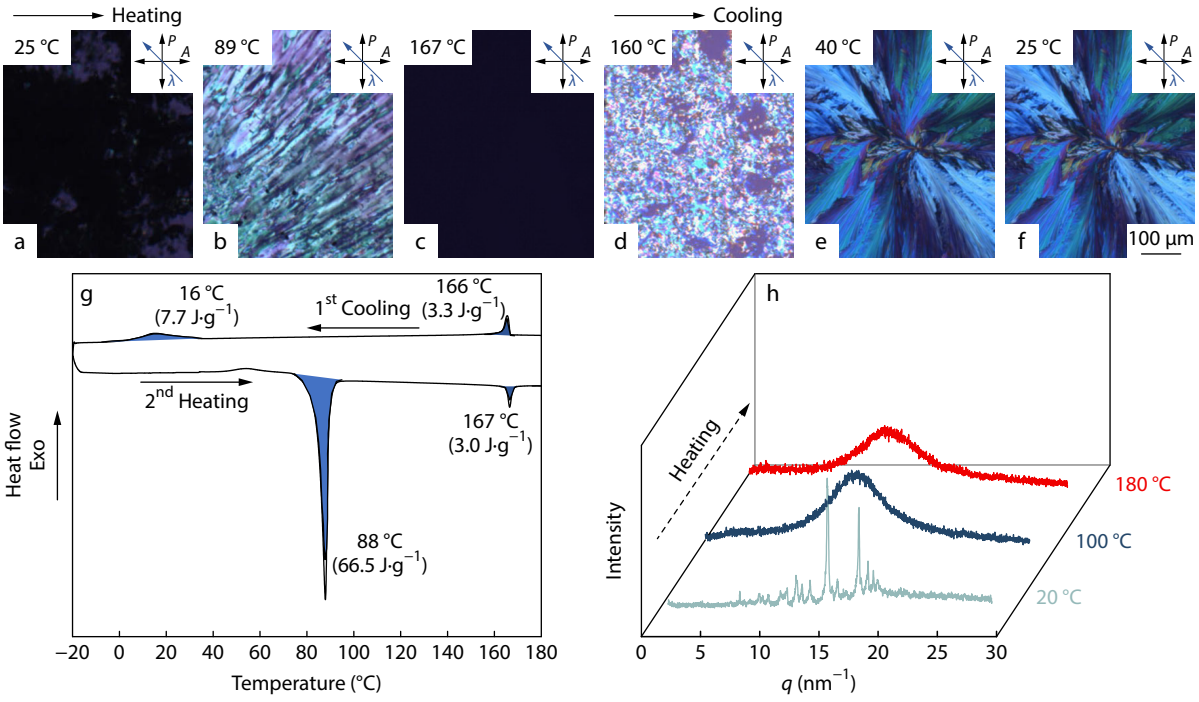

Fig. 2 (a–f) POM images of E6M during heating and cooling, in which the heating was implemented at a ramp rate of 3 °C·min^{-1} from 25 °C to 170 °C while the cooling was exerted at a ramp rate of 2 °C·min^{-1}. *A*: analyzer, *P*: polarizer, λ: phase retarder. (g) DSC curves of the E6M during the first cooling and second heating at a ramp rate of 5 °C·min^{-1} between −20 and 180 °C; (h) T-WAXS patterns of E6M when heating.

https://doi.org/10.1007/s10118-024-3110-z

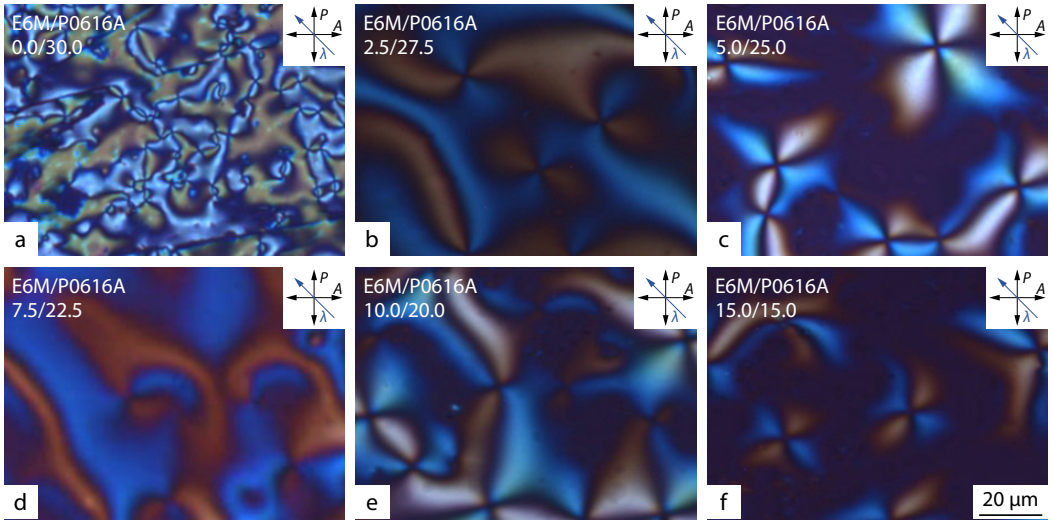

Fig. 3 POM images with different mass ratios of E6M/P0616A when the temperature falls below the clearing point. The mass ratios of E6M/P0616A: (a) 0.0/30.0; (b) 2.5/27.5; (c) 5.0/25.0; (d) 7.5/22.5; (e) 10.0/20.0; (f) 15.0/15.0.

at 160 °C and turn to focal conic below the temperature of 40 °C (Figs. 2d–2f), which may be driven by the transition from LC phase to crystalline phase. DSC results supported the POM observations (Fig. 2g). Two exothermal peaks can be observed upon cooling, which are at 166 and 16 °C, respectively. The first peak indicates isotropic-nematic phase transition, while the second with a small enthalpy of 7.7 J·g^{-1} may be accompanied by slow crystallization. In sharp contrast, there is a large endothermal peak (enthalpy: 66.5 J·g^{-1}) at 88 °C upon heating, which was the sign of E6M melting. The small endothermal peak at 167 °C indicated the nematic-isotropic phase transition and the temperature was referred as the clearing point. To further confirm the LC phase of E6M, T-WAXS analysis was exerted, and the results showed that E6M was crystalline at 20 °C while in nematic phase at 100 °C with the sharp reflection peaks fading to a broad halo (Fig. 2h).

Influence of E6M on the Phase Transition Behavior of P0616A

The LC characteristic of E6M would facilitate the miscibility with the nematic P0616A for holographic recording.[30] As shown in Fig. S6 (in ESI), homogeneous E6M/P0616A mixtures were ready *via* simple mixing with varying mass ratios of 0.0/30.0, 2.5/27.5, 5.0/25.0, 7.5/22.5, 10.0/20.0 and 15.0/15.0, respectively. As displayed in Fig. 3, with the increase of E6M content, the characteristic schlieren textures of nematic LCs were gradually enlarged, implying the formation of larger LC domains. Interestingly, the nematic LC tended to be more ordered according to the color change of schlieren textures, and cyan-blue and brown colors were shown when increasing the E6M loading. Basically, the former color indicates a parallel molecular alignment with respect to the slow axis of the phase retarder while the latter shows a perpendicular alignment.[30,48]

The preferred molecular orientation of P0616A by E6M can be described by the order parameter:[49,50]

$$S = \frac{K(T_C - T)}{T_C} \quad (2)$$

where T_C and T denote the clearing point of the LC and a temperature below the clearing point, respectively, and K is a proportional constant. This temperature dependent order parameter tells us that with the increase of clearing point, the more ordered of LC molecules would be at an observed temperature lower than the clearing point. Interestingly, with the increase of mass ratio of E6M to P0616A from 0.0/30.0 to 15.0/15.0, the clearing point of the LC mixtures is found to increase from 58.1

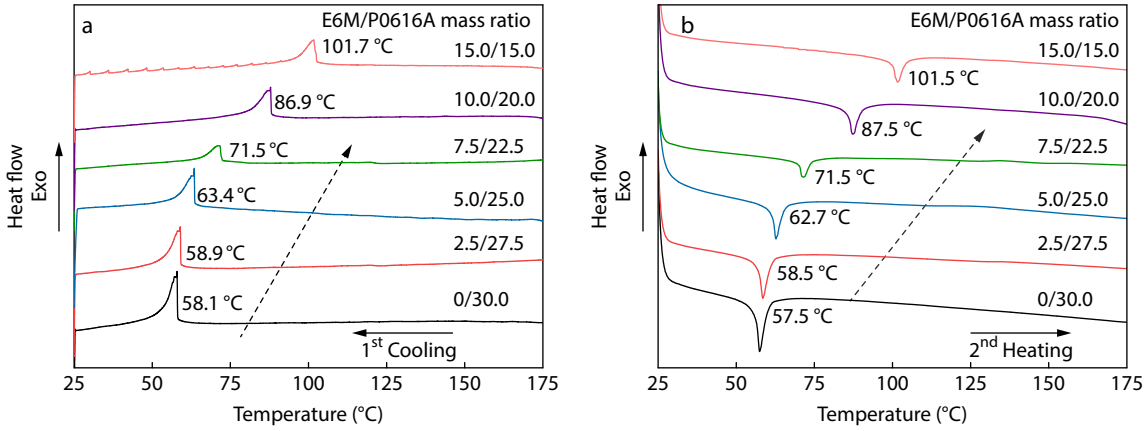

Fig. 4 DSC curves of the E6M/P0616A mixtures at a ramp rate of 5 °C·min^{-1}: (a) during the first cooling, (b) during the second heating.

https://doi.org/10.1007/s10118-024-3110-z

℃ to 101.7 ℃ during the first cooling and arise from 57.5 ℃ to 101.5 ℃ during the second heating (Fig. 4). The ~76.5% increment of nematic-isotropic phase transition temperatures clearly demonstrates the increased molecular alignment and long-range orientation order of LC mixtures by E6M.

Influences of E6M on the Reaction Kinetics and Holographic Performance

The increased clearing point of LC mixtures by E6M might facilitate the LC nucleation during holographic patterning, which then may affect the photopolymerization kinetics, phase separation structures and holographic performance. By evaluating the photopolymerization kinetics using the previously reported method based on FTIR,[15,47] we noted that the photopolymerization was generally accelerated by E6M and the double bond conversion increased 6% when adding 15 wt% of E6M (Fig. 5).

The introduction of E6M was also found to boost the holographic performance. We first evaluated the influences of E6M on the diffraction efficiency, η, and refractive index modulation, n_1. As shown in Fig. 6(a), a 633 nm laser was employed to probe the transmission gratings in a non-destructive modality, where p-polarization meant an electric field of the probe beam was parallel to the plane of the incidence

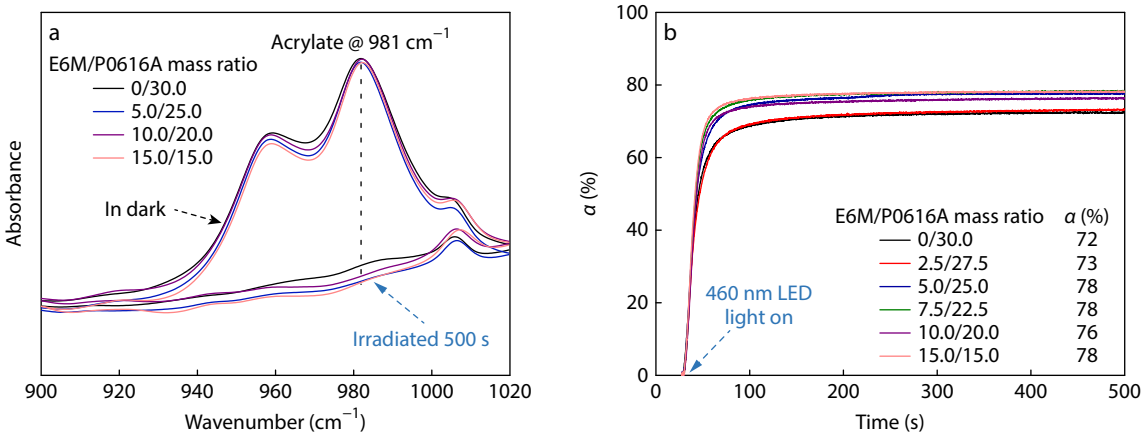

Fig. 5 (a) Representative FTIR absorptions of the holographic mixture at 0 s and 500 s of light irradiation time; (b) Calculated double bond conversion (α) versus light irradiation time for homogeneous mixtures containing varied mass ratio of E6M/P0616A. Light wavelength: 460 nm, intensity: 2.0 mW·cm^{-2}.

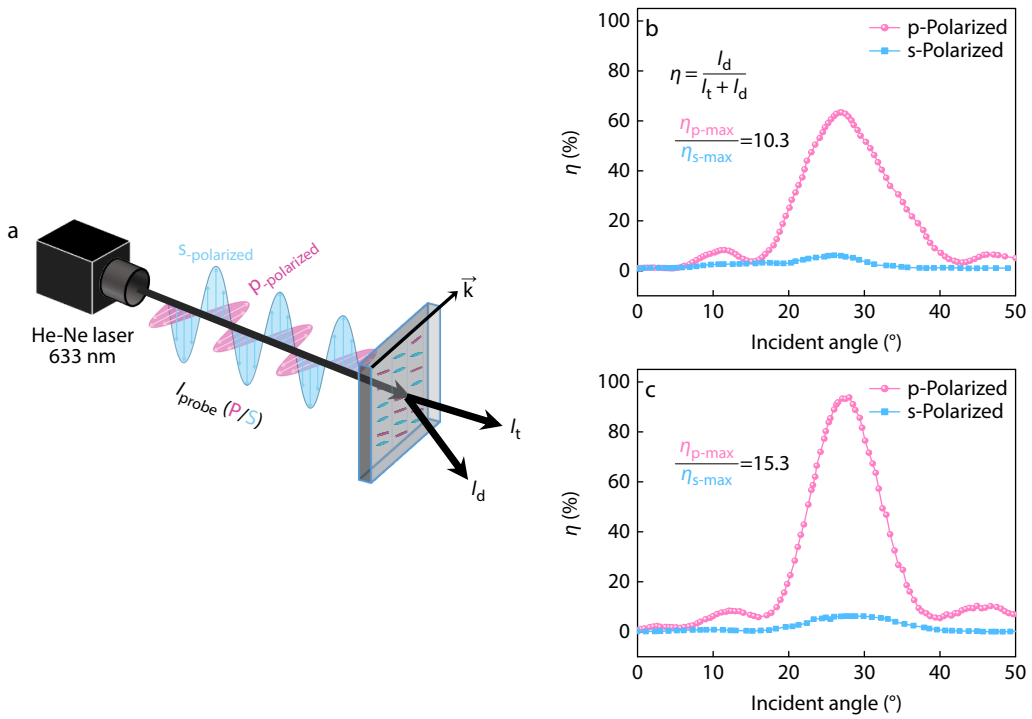

Fig. 6 (a) Schematic illustration on the characterization of p- and s-polarization dependent diffraction efficiency of the formed transmission gratings, in which I_t is the transmission intensity and I_d is diffraction intensity, I_{probe} is probing light intensity and $\vec{k}$ is grating vector, respectively. (b, c) Diffraction efficiency (η) against the incident angle of the probing beam for the transmission gratings (thickness: 5 μm): (b) the E6M/P0616A mass ratio is 0.0/30.0, (c) the E6M/P0616A mass ratio is 5.0/25.0.

https://doi.org/10.1007/s10118-024-3110-z

while s-polarization had an electric field in the vertical. When probed from the Bragg angle, the holographic gratings display a maximum diffraction intensity, the diffraction efficiency can be calculated using the equation shown in Fig. 6(b).[26,51] Interestingly, the formulated transmission gratings with E6M showed a large dependence on p-polarization of the probe laser, implying the preferred parallel alignment of LC molecules along with grating vector. In addition, the ratio of p-polarized diffraction efficiency to the s-polarized was found to increase by 48.5% (*i.e.*, from 10.3 to 15.3), with an augmentation of E6M/P0616A mass ratio from 0.0/30.0 to 5.0/25.0 (Fig. 6c). These results further support the conclusion that the LC alignment can be promoted by E6M.

For a transmission holographic grating without overmodulation, a high diffraction efficiency is given by the large n_1,[52]

$$n_1 = \frac{\arcsin\left(\eta^{0.5}\right)\cos\theta_B\lambda_{probe}}{\pi d} \quad (3)$$

where λ_{probe} is the wavelength of probe laser, θ_B denotes the Bragg angle, and d represents the grating thickness.[53,54] As displayed in Fig. 7(a), n_1 is generally increased with an augmentation of E6M content and could reach 0.046 @ 633 nm at the mass ratio of 5.0/25.0 for E6M/P0616A. In comparison with the control without E6M, the n_1 exhibits a great increasement by 44%. Nevertheless, the haze of holographic gratings was found to increase with an augmentation of the mass ratio, and holographic gratings were hard to fabricate when further increasing the mass ratio more than 15.0/15.0 as E6M could not be completely dissolved (Fig. S7 in ESI). Excitingly, the formulated composite gratings in this work can also show a high optical quality with a small haze at 5.0% (Fig. 7b). To further boost the n_1, the irradiation intensity for each coherent laser beam was further increased, and eventually a high n_1 up to 0.050 @ 633 nm was achieved while the haze was maintained at 5.0% when the laser intensity was 3 mW·cm^{-2} (Figs. 7c and 7d).

To get a deeper insight into the mechanism for the boosted n_1 by E6M, the segregation degree (SD) was evaluated according to the following equation:[13,38,55]

$$n_1 = SD \times f_{LC} \times (n_{LC} - n_P) \quad (4)$$

where f_{LC} was the LC volume fraction (29.4 % in this work), SD signified the degree of phase separation, n_{LC} and n_P denoted the refractive index of LC and polymer, respectively. Due to the lack of viable methods to characterize the SD by experiments apart from diffraction efficiency,[13] the SD can be roughly estimated from the phase separation structures. As shown in Fig. 8, the AFM measured grating depth was 123±5, 148±8, 123±11, 116±25, 134±14 and 127±8 nm, respectively, when increasing the mass ratio of E6M/P0616A from 0.0/30.0 to 15.0/15.0, which implies insignificant changes of phase separation structures and SD. This result supports that the increased n_1 by E6M is primari-

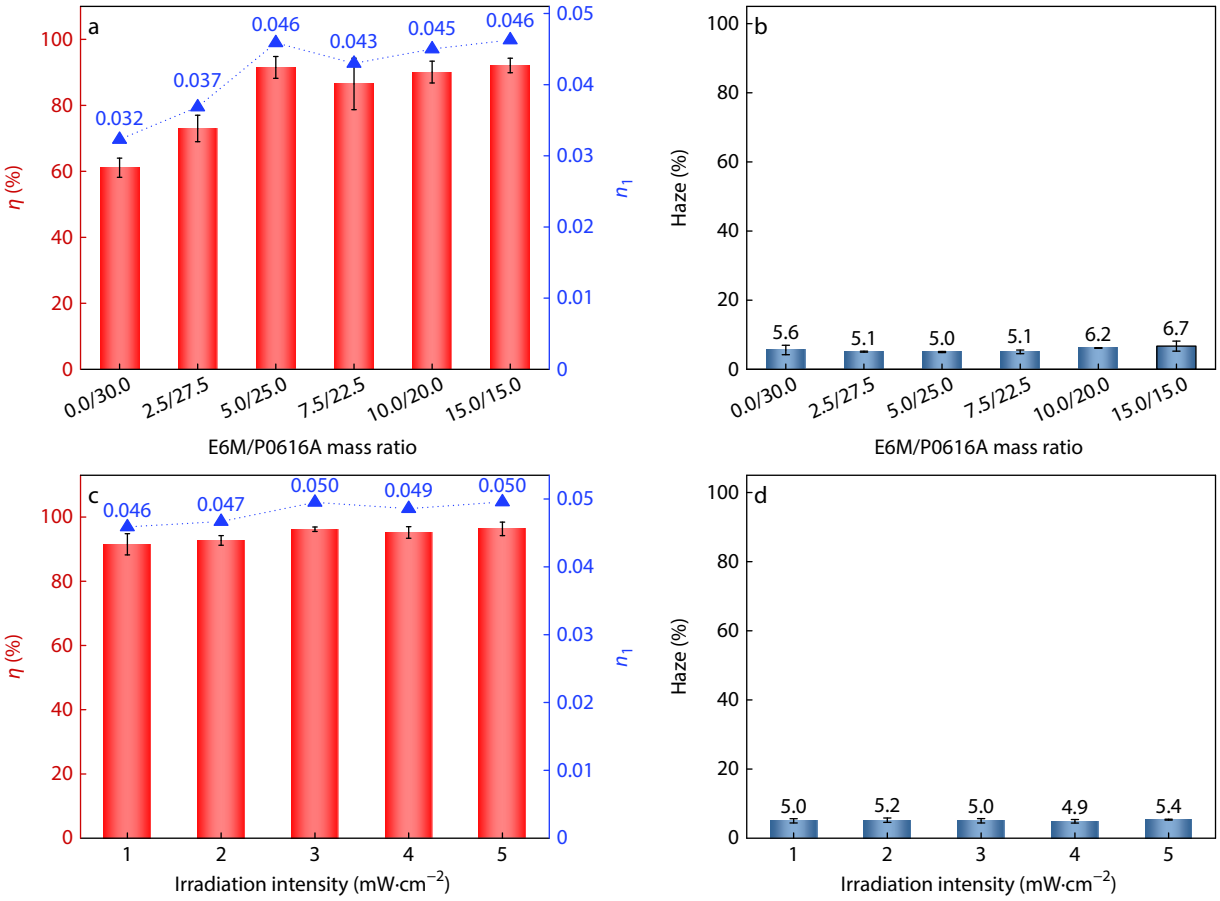

Fig. 7 (a) p-Polarized diffraction efficiency and refractive index modulation and (b) haze for the composite gratings (thickness: 5 μm) with varied mass ratio of E6M/P0616A; (c) p-Polarized diffraction efficiency and refractive index modulation and (d) haze for the composite gratings against the irradiation intensity when the E6M/P0616A mass ratio was 5.0/25.0.

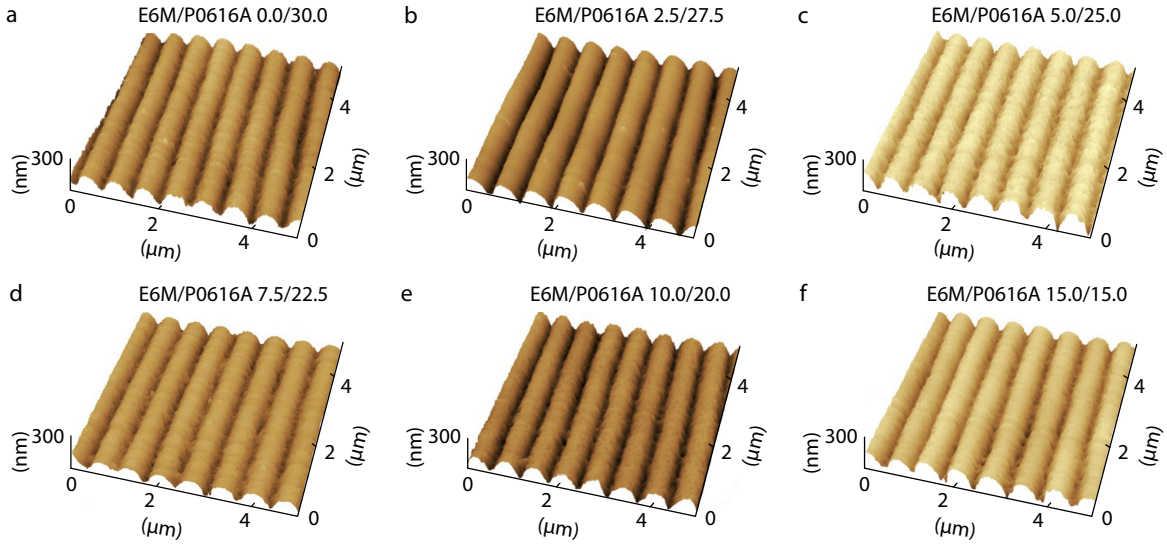

Fig. 8 AFM profiles of the composite gratings with different mass ratios of E6M/P0616A after removing LCs with *n*-hexane. The mass ratios: (a) 0.0/30.0; (b) 2.5/27.5; (c) 5.0/25.0; (d) 7.5/22.5; (e) 10.0/20.0; (f) 15.0/15.0.

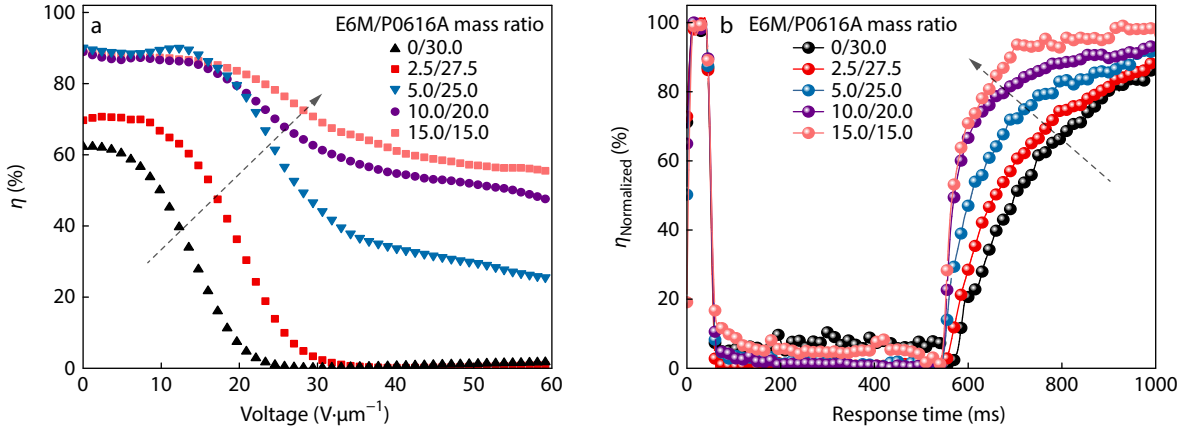

Fig. 9 (a) Diffraction efficiency versus applied alternating voltage; (b) Normalized diffraction efficiency against response time for the composite gratings with varying mass ratios of E6M/P0616A.

ly ascribed to the strengthened LC alignment along with grating vector.[56] As we all know, the LC refractive index in the long axis is much higher than that in the short axis, thus the preferred LC alignment can afford a high refractive index contrast between the LC-rich and polymer-rich regions. It is also worth noting that uniform LC alignment could downscale the differences in order parameter between different LC domains and consequently could reduce the light scattering losses and improve the optical quality.[39] Although similar results can be obtained by adding MPEB (Figs. S8–S13 in ESI), E6M exhibits far beyond performance.

Effect of E6M on the Electro-optic Response of Holographic Gratings

Fig. 9(a) displays the diffraction efficiency of composite gratings against applied alternative voltage. As clearly shown, the diffraction efficiency is declined when applying an alternating voltage from 0 V to 300 V with an interval of 0.5 V, and eventually levels off. This is due to the reorientation of LC molecules with positive dielectric constants along with the electric field can decrease the refractive index contrast between polymer-rich and LC-rich phases. With an augmentation of the mass ratio of E6M/P0616A from 0.0/30.0 to 5.0/25.0, the calculated threshold voltage[38,57] increases from 7.4 V·μm^{-1} to 17.5 V·μm^{-1}, and the saturated voltage increases from 20.2 V·μm^{-1} to 44.5 V·μm^{-1}. With the mass ratio further increasing to 15.0/15.0, both the threshold and saturated voltages are maintained at higher values. For the composite gratings with scaffolding morphology, the increased driving voltage is mainly ascribed to the boosted interfacial interaction between polymer-rich and LC-rich region.[38] This is in good agreement with shortened decay time from 457 ms to 143 ms when turning off the electric field (Fig. 9b). The results are reasonable as more and more LC molecules would be directly anchored at the interface when the LC molecules are aligned along with grating vector as illustrated in Fig. 1. Under such a condition, interfacial actions rather than bend elastic force of LCs would govern the electro-optic response behaviors.

CONCLUSIONS

In summary, we demonstrated a viable approach to boost refractive index modulation of holographic polymer nanocom-

posites by doping E6M. E6M was found to benefit the LC alignment within the LC-rich regions of composite gratings according to POM and DSC characterizations, which could not only enlarge the refractive index difference between the polymer-rich and LC-rich regions, but also could constrain the light scattering loss. Therefore, a high refractive index modulation of 0.050 @ 633nm and low haze of 5.0% could be obtained, enabling a high diffraction efficiency of 96.2% for 5 μm-thick transmission gratings. In comparison with other work by solely introducing high refractive index LCs, the major advantage of this approach is that the significant light scattering can be depressed by uniform LC ordering within the LC-rich domains. Therefore, high optical quality composite gratings can be promising to be utilized as HOEs for future advanced AR applications.

Conflict of Interests

The authors declare no interest conflict.

Electronic Supplementary Information

Electronic supplementary information (ESI) is available free of charge in the online version of this article at http://doi.org/10.1007/s10118-024-3110-z.

Data Availability Statement

The data that support the findings of this study are available from the corresponding author upon reasonable request. The author's contact information: hypeng@hust.edu.cn.

ACKNOWLEDGMENTS

This work was financially supported by the National Natural Science Foundation of China (Nos. 52122316, 52073108 and 52233005) and the Innovation and Talent Recruitment Base of New Energy Chemistry and Device (No. B21003). Analytical assistance from HUST Analytical & Testing Center, and Core Facilities of Life Sciences are also appreciated.

REFERENCES

1 Li, X.; Yi, W.; Chi, H. L.; Wang, X.; Chan, A. P. C. A critical review of virtual and augmented reality (VR/AR) applications in construction safety. *Autom. Constr.* **2018**, *86*, 150–162.
2 Zhan, T.; Yin, K.; Xiong, J. H.; He, Z. Q; Wu, S. T. Augmented reality and virtual reality displays: perspectives and challenges. *iScience* **2020**, *23*, 101397.
3 Martinez-Millana, A.; Bayo-Monton, J. L.; Lizondo, A.; Fernandez-Llatas, C.; Traver, V. Evaluation of google glass technical limitations on their integration in medical systems. *Sensors* **2016**, *16*, 2142.
4 Talha, M. M.; Chang, J.; Wang, Y. T.; Zhang, T. C.; Cheng, D. W.; Hui, Sun. Z. Design, tolerancing and stray light analyses of a freeform HMD optical system. *Optik* **2010**, *121*, 750–755.
5 Cholewiak, S. A.; Basgoze, Z.; Cakmakci, O.; Hoffman, D. M.; Cooper, E. A. A perceptual eyebox for near-eye displays. *Opt. Express* **2020**, *28*, 38008–38028.
6 Yin, K.; He, Z. Q.; Xiong, J. H.; Zou, J. Y.; Li, K.; Wu, S. T. Virtual reality and augmented reality displays: advances and future perspectives. *J. Phys. Photonics* **2021**, *3*, 022010.
7 Ni, M. L.; Yang, S.; Zhou, X. P.; Peng, H. Y.; Song, Q. M.; Xie, X. L. Holographic polymer materials for VR/AR applications. *Acta Polymerica Sinica* (in Chinese) **2023**, *54*, 418–431.
8 Fang, W.; Chen, L. X.; Zhang, T. N.; Chen, C. J.; Teng, Z.; Wang, L. H. Head-mounted display augmented reality in manufacturing: a systematic review. *Robot. Comput. Integr. Manuf.* **2023**, *83*, 102567.
9 Amitai, Y. In P-27: a two-dimensional aperture expander for ultra-compact, high-performance head-worn displays. *SID Symp. Dig. Tech. Pap.* **2005**, *36*, 360–363.
10 Shen, Z. W.; Zhang, Y. N.; Liu, A.; Weng, Y. S.; Li, X. H. Volume holographic waveguide display with large field of view using an Au-NPs dispersed acrylate-based photopolymer. *Opt. Mater. Express* **2020**, *10*, 312–322.
11 Kress, B. C.; Pace, M. Holographic optics in planar optical systems for next generation small form factor mixed reality headsets. *Light Adv. Manuf.* **2022**, *3*, 771–801.
12 Xiong, J. H.; Tan, G.; Zhan, T.; Wu, S. T. Breaking the field-of-view limit in augmented reality with a scanning waveguide display. *OSA Continuum* **2020**, *3*, 2730–2740.
13 Wei, W.; Chen, G. N.; Li, S.; Zhou, X. P.; Peng, H. Y.; Xie, X. L; Mai, Y. W. Computational insight into phase separation of a thiol-ene photopolymer with liquid crystals for holography by dissipative particle dynamics simulation. *Macromolecules* **2023**, *56*, 5457–5469.
14 Ni, M. L.; Chen, G. N.; Wang, Y.; Peng, H. Y.; Liao, Y. G.; Xie, X. L. Holographic polymer nanocomposites with ordered structures and improved electro-optical performance by doping POSS. *Compos. Part B-Eng.* **2019**, *174*, 107045.
15 Chen, G. N.; Wei, W.; Li, S.; Zhou, X. P.; Li, Z. A.; Peng, H. Y.; Xie, X. L. Liquid crystal-assisted manufacturing of flexible holographic polymer nanocomposites for high-security level anticounterfeiting. *Mater. Chem. Front.* **2022**, *6*, 3531–3542.
16 Zhao, W.; De Haan, L. T.; Broer, D. J.; Zhang, Y.; Lv, P. R.; Zhou, G. F. Photopolymerization-enforced stratification in liquid crystal materials. *Prog. Polym. Sci.* **2021**, *114*, 101365.
17 Saeed, M. H.; Zhang, S. F.; Cao, Y. P.; Zhou, L.; Hu, J. M.; Muhammad, I.; Xiao, J. M.; Zhang, L. Y.; Yang, H. Recent advances in the polymer dispersed liquid crystal composite and its applications. *Molecules* **2020**, *25*, 5510.
18 Guo, S. M.; Liang, X.; Zhang, C. H.; Chen, M.; Shen, C.; Zhang, L. Y.; Yuan, X.; He, B. F.; Yang, H. Preparation of a thermally light-transmittance-controllable film from a coexistent system of polymer-dispersed and polymer-stabilized liquid crystals. *ACS Appl. Mater. Interfaces* **2017**, *9*, 2942–2947.
19 White, T. J.; Natarajan, L. V.; Tondiglia, V. P.; Bunning, T. J.; Guymon, C. A. Polymerization kinetics and monomer functionality effects in thiol-ene polymer dispersed liquid crystals. *Macromolecules* **2007**, *40*, 1112–1120.
20 Xiong, J. H.; Wu, S. T. Planar liquid crystal polarization optics for augmented reality and virtual reality: from fundamentals to applications. *eLight* **2021**, *1*, 3.
21 Xiong, J. H.; Chen, R.; Wu, S. T. Device simulation of liquid crystal polarization gratings. *Opt. Express* **2019**, *27*, 18102–18112.
22 Lee, Y. H.; Yin, K.; Wu, S. T. Reflective polarization volume gratings for high efficiency waveguide-coupling augmented reality displays. *Opt. Express* **2017**, *25*, 27008–27014.
23 Liu, Y. J.; Sun, X. W. Holographic polymer-dispersed liquid crystals: materials, formation, and applications. *Adv. OptoElectron.* **2008**, *2008*, 684349.
24 Jiang, H. D.; Cai, W. F.; Li, K.; Cheng, M.; Kumar, V.; Yin, Z.; Gérard, D.; Luo, D.; Mu, Q. Q.; Liu, Y. J. Holographically fabricated, highly reflective nanoporous polymeric distributed bragg reflectors with red, green, and blue colors. *Chin. Opt. Lett.* **2020**, *18*, 080007.
25 White, T. J.; Natarajan, L. V.; Tondiglia, V. P.; Lloyd, P. F.; Bunning, T. J.; Guymon, C. A. Monomer functionality effects in the

formation of thiol-ene holographic polymer dispersed liquid crystals. *Macromolecules* **2007**, *40*, 1121–1127.
26 Hu, Y. X.; Hao, X. T.; Xu, L.; Xie, X. L.; Xiong, B. J.; Hu, Z. B.; Sun, H. T.; Yin, G. Q.; Li, X. P.; Peng, H. Y.; Yang, H. B. Construction of supramolecular liquid-crystalline metallacycles for holographic storage of colored images. *J. Am. Chem. Soc.* **2020**, *142*, 6285–6294.
27 Peng, H. Y.; Bi, S. G.; Ni, M. L.; Xie, X. L.; Liao, Y. G.; Zhou, X. P.; Xue, Z. G.; Zhu, J. T.; Wei, Y.; Bowman, C. N.; Mai, Y. W. Monochromatic visible light "photoinitibitor": Janus-faced initiation and inhibition for storage of colored 3D images. *J. Am. Chem. Soc.* **2014**, *136*, 8855–8858.
28 Chen, G. N.; Ni, M. L.; Peng, H. Y.; Huang, F. H.; Liao, Y. G; Wang, M. K.; Zhu, J. T.; Roy, V. A. L.; Xie, X. L. Photoinitiation and inhibition under monochromatic green light for storage of colored 3D images in holographic polymer-dispersed liquid crystals. *ACS Appl. Mater. Interfaces* **2017**, *9*, 1810–1819.
29 Peng, H. Y.; Yu, L.; Chen, G. N.; Bohl, T. W.; Ye, Y. S.; Zhou, X. P.; Xue, Z. G.; Roy, V. A. L.; Xie, X. L. Low-voltage-driven and highly-diffractive holographic polymer dispersed liquid crystals with spherical morphology. *RSC Adv.* **2017**, *7*, 51847–51857.
30 Peng, H. Y.; Yu, L.; Chen, G. N.; Xue, Z. G.; Liao, Y. G.; Zhu, J. T.; Xie, X. L.; Smalyukh, I. I.; Wei, Y. Liquid crystalline nanocolloids for the storage of electro-optic responsive images. *ACS Appl. Mater. Interfaces* **2019**, *11*, 8612–8624.
31 Wang, Y. X.; Liu, Y.; Hao, X. T.; Zhou, X. P.; Peng, H. Y.; Shen, Z. H.; Smalyukh, I. I.; Xie, X. L.; Yang, B. Supramolecular liquid crystal carbon dots for solvent-free direct ink writing. *Adv. Mater.* **2023**, *35*, 2303680.
32 Yao, M.; Zhao, Y.; Zhou, X. P.; Li, Z. A.; Peng, H. Y.; Xie, X. L. Orthogonal integration of holographic and fluorescent dual images based on energy transfer from liquid crystals to a photocleavable AIEgen. *J. Mater. Chem. C* **2023**, *11*, 3504–3512.
33 Zhao, X. Y.; Zhao, Y.; Li, M.-D.; Li, Z. A.; Peng, H. Y.; Xie, T.; Xie, X. L. Efficient 3D printing *via* photooxidation of ketocoumarin based photopolymerization. *Nat. Commun.* **2021**, *12*, 2873.
34 Zhao, Y.; Peng, H. Y.; Zhou, X. P.; Li, Z. A.; Xie, X. L. Interfacial aie for orthogonal integration of holographic and fluorescent dual-thermosensitive images. *Adv. Sci.* **2022**, *9*, 2105903.
35 Zola, R. S.; Bisoyi, H. K.; Wang, H.; Urbas, A. M.; Bunning, T. J.; Li, Q. Dynamic control of light direction enabled by stimuli-responsive liquid crystal gratings. *Adv. Mater.* **2019**, *31*, 1806172.
36 Jonathan, D. W.; Alastair, J. G.; Milan, M. P. In Wide field of view multiplexed photopolymer consumer AR displays. *Proc.SPIE* **2020**, *11310*, 148–159.
37 Jonathan, D. W.; Shibu, A.; Milan, M. P. In DigiLens holographic photopolymers for wide angle AR waveguides. *Proc.SPIE* **2020**, *11367*, 54–63.
38 Peng, H. Y.; Chen, G. N.; Ni, M. L.; Yan, Y.; Zhuang, J. Q.; Roy, V. A. L.; Li, R. K. Y.; Xie, X. L. Classical photopolymerization kinetics, exceptional gelation, and improved diffraction efficiency and driving voltage in scaffolding morphological H-PDLCs afforded using a photoinitibitor. *Polym. Chem.* **2015**, *6*, 8259–8269.
39 Zheng, Z. G.; Zhou, L.; Shen, D.; Xuan, L. Holographic polymer-dispersed liquid crystal grating with low scattering losses. *Liq. Cryst.* **2012**, *39*, 387–391.
40 Mallon, J. J.; Adams, P. M. Synthesis and characterization of novel epoxy monomers and liquid crystal thermosets. *J. Polym. Sci., Part A: Polym. Chem.* **1993**, *31*, 2249–2260.
41 Shen, W. B.; Wang, L.; Chen, G.; Li, C. X.; Zhang, L. Y.; Yang, Z.; Yang, H. A facile route towards controllable electric-optical performance of polymer-dispersed liquid crystal *via* the implantation of liquid crystalline epoxy network in conventional resin. *Polymer* **2019**, *167*, 67–77.
42 Hu, Y. F.; Kowalski, B. A.; Mavila, S.; Podgórski, M.; Sinha, J.; Sullivan, A. C.; McLeod, R. R.; Bowman, C. N. Holographic photopolymer material with high dynamic range (Δ*n*) *via* thiol-ene click chemistry. *ACS Appl. Mater. Interfaces* **2020**, *12*, 44103–44109.
43 Zhang, X. M.; Yao, W. J.; Zhou, X. P.; Wu, W.; Liu, Q. K.; Peng, H. Y.; Zhu, J. T.; Smalyukh, I. I.; Xie, X. L. Holographic polymer nanocomposites with simultaneously boosted diffraction efficiency and upconversion photoluminescence. *Compos. Sci. Technol.* **2019**, *181*, 107705.
44 Hu, Y.; Podgórski, M.; Mavila, S.; Sinha, J.; Fairbanks, B. D.; McLeod, R. R.; Bowman, C. N. Dynamic polymer binder with light-regulated molecular weight *via* addition-fragmentation chain transfer for holographic recording. *Macromolecules* **2023**, *56*, 2536–2541.
45 Sarkar, M. D.; Gill, N. L.; Crawford, G. P. Effect of monomer functionality on the morphology and performance of the holographic transmission gratings recorded on polymer dispersed liquid crystals. *Macromolecules* **2003**, *36*, 630–638.
46 Ni, M. L.; Peng, H. Y.; Xie, X. L. Structure regulation and performance of holographic polymer dispersed liquid crystals. *Acta Polymerica Sinica* (in Chinese) **2017**, 1557-1573.
47 Zhao, X. Y.; Sun, S. S.; Zhao, Y.; Liao, R. Z.; Li, M. D.; Liao, Y. G.; Peng, H. Y.; Xie, X. L. Effect of ketyl radical on the structure and performance of holographic polymer/liquid-crystal composites. *Sci. China Mater.* **2019**, *62*, 1921–1933.
48 Gim, M. J.; Beller, D. A.; Yoon, D. K. Morphogenesis of liquid crystal topological defects during the nematic-smectic A phase transition. *Nat. Commun.* **2017**, *8*, 15453.
49 Saupe, A. Kernresonanzen in kristallinen flussigkeiten und in kristallinflussigen losungen. Teil I. *Z. Naturforsch. A* **1964**, *19*, 161–171.
50 Gao, H. J. *Liquid Crystal Chemistry*, Tsinghua University Press, Beijing, **2011**, P. 12.
51 Vardanyan, K. K.; Qi, J.; Eakin, J. N.; De Sarkar, M.; Crawford, G. P. Polymer scaffolding model for holographic polymer-dispersed liquid crystals. *Appl. Phys. Lett.* **2002**, *81*, 4736–4738.
52 Sakhno, O. V.; Goldenberg, L. M.; Stumpe, J.; Smirnova, T. N. Surface modified ZrO_2 and TiO_2 nanoparticles embedded in organic photopolymers for highly effective and UV-stable volume holograms. *Nanotechnology* **2007**, *18*, 105704.
53 Kogelnik, H. Coupled wave theory for thick hologram gratings. *Bell. Syst. Tech. J.* **1969**, *48*, 2909–2947.
54 Hu, Y. F.; Mavila, S.; Podgórski, M.; Kowalski, J. E.; McLeod, R. R.; Bowman, C. N. Manipulating the relative rates of reaction and diffusion in a holographic photopolymer based on thiol-ene chemistry. *Macromolecules* **2022**, *55*, 1822–1833.
55 Sakhno, O. V.; Goldenberg, L. M.; Stumpe, J.; Smirnova, T. N. Effective volume holographic structures based on organic–inorganic photopolymer nanocomposites. *J. Opt. A: Pure Appl. Opt.* **2009**, *11*, 024013.
56 Mavila, S.; Sinha, J.; Hu, Y. F.; Podgórski, M.; Shah, P. K.; Bowman, C. N. High refractive index photopolymers by thiol-yne “click” polymerization. *ACS Appl. Mater. Interfaces* **2021**, *13*, 15647–15658.
57 Bunning, T. J.; Natarajan, L. V.; Tondiglia, V. P.; Sutherland, R. L. Holographic polymer-dispersed liquid crystals (H-PDLCs). *Annu. Rev. Mater. Sci.* **2000**, *30*, 83–115.

https://doi.org/10.1007/s10118-024-3110-z